Biogeosciences Open Access
EGU
Discussions

Technical Note: Novel triple O₂-sensor aquatic eddy covariance instrument with improved time-shift correction reveals central role of microphytobenthos for carbon cycling in coral reef sands

5   Alireza Merikhi[1], Peter Berg[2], Markus Huettel[1]

[1] Department of Earth, Ocean and Atmospheric Science, Florida State University, Tallahassee, FL 32306-4520, USA
[2] Department of Environmental Sciences, University of Virginia, Charlottesville, VA 22904-4123, USA

Correspondence to: Markus Huettel (mhuettel@fsu.edu)

Abstract. The aquatic eddy covariance technique stands out as a method for benthic O₂-flux measurements because it measures

10   non-invasively, but in the conventional instruments, the spatial separation of the measuring locations of the velocity and O₂ sensors causes a time-shift that can be substantial and difficult to correct. Here we introduce a triple O₂-sensor-eddy covariance instrument (3OEC) that by positioning of the O₂-sensors around the flow measuring volume allows eliminating these time-shifts through signal averaging. The new instrument was used to determine O₂-production and consumption in an energetic coastal environment with highly permeable coral reef sands colonized by microphytobenthos. The measurement at ~10 m

15   water depth revealed O₂-fluxes that range among the highest reported for marine sediments despite relatively low organic content of the water and coarse sediment, indicating a central role of microphytobenthos for the carbon and nutrient cycling in the coral sand. High light utilization efficiency of the microphytobenthos and bottom currents increasing pore water exchange facilitated the high benthic production and respiration. The measurements documented a gradual transfer of the flux signal from the small turbulence generated at the sediment water interface to the larger wave-dominated eddies of the overlying water

20   column with a delay influenced by the memory effect of eddies. These results demonstrate that the 3OEC can improve the precision of the flux measurements, including measurements in environments considered challenging for this technique, and thereby produce novel insights into the mechanisms that control flux. We consider the fluxes produced by this instrument for the permeable reef sands the most realistic achievable with present day technology.

1 Introduction

25   This study introduces a new eddy covariance instrument and demonstrates its functionality through a measuring series addressing the metabolism of permeable coral reef sands. Warm water coral reefs are rapidly deteriorating due to ocean warming, acidification and eutrophication (Hughes et al., 2018;Stuart-Smith et al., 2018;Fogarty and Marhaver, 2019), and understanding the cycles of matter in these reefs is prerequisite for assessing their functioning, health and fate (Pawlik et al., 2016;Albright et al., 2018;Deschaseaux et al., 2019). Carbonate sediments are an integral part of reef environments and present

30   sites of organic and inorganic carbon production and consumption (Eyre et al., 2018;Santos et al., 2011;Cyronak et al., 2013). As warm water coral reefs grow in shallow, high-energy environments, these sediments typically are dominated by coarse

sands (Yahel et al., 2002;Harris et al., 2015) that are colonized by microphytobenthos (Werner et al., 2008;Jantzen et al., 2013). Benthic chamber incubations demonstrated high biogeochemical activity in these sediments despite their relatively low content of organic matter (Wild et al., 2004c;Eyre et al., 2008;Glud et al., 2008). Owing to the rapid pore water exchange facilitated

35   by the high permeability of these sands, biogeochemical processes in the sediment surface layers can respond almost instantly to changes in flow, degradable organic matter input, and light (Huettel et al., 2014). These dynamics are difficult to quantify accurately with methods that change the light that reaches the sand surface and isolate the enclosed sediment and water. Although production and mineralization processes in the carbonate sands may play a central role for the functioning of coral reef ecosystems, magnitudes and dynamics of the benthic fluxes thus are not well understood.

40

To address this issue, we developed and deployed an aquatic eddy covariance instrument that allows improved O_2-flux measurements in highly energetic environments. Benthic O_2-flux is a good proxy for the benthic production and respiration (Berg et al., 2013;Glud, 2008) and it can be measured in-situ at high temporal resolution with the aquatic eddy covariance technique (Berg et al., 2003). This technique derives flux by averaging the turbulent vertical advective transport of O_2 above

45   the sediment over time (Berg et al., 2003;Lorrai et al., 2010;McGinnis et al., 2008b). Since the measured flux signals originate from the seafloor upstream of the instrument (termed "footprint"), the technique does not interfere with the natural flow and light fields, or disturb the benthic sedimentary community (Berg et al., 2003;Lorrai et al., 2010;McGinnis et al., 2008b;Huettel et al., 2020). The eddy covariance method thus can produce realistic benthic flux data in highly dynamic coastal ecosystems as coral reefs (Long et al., 2013;Long, 2021;Huettel et al., 2020), however, small uncertainties in the alignment of the signals

50   recorded by the current and solute sensors can result in large errors of the calculated fluxes. Conventional eddy covariance instruments measure current velocities with an acoustic Doppler velocimeter (ADV), and O_2 with a fast-responding electrochemical or optical O_2 sensor (Kuwae et al., 2006;Berg et al., 2003;Reimers et al., 2012;Attard et al., 2016;Donis et al., 2016;Glud et al., 2010;McGinnis et al., 2014;Lorke et al., 2013;Huettel et al., 2020). Although the covariance calculations require measurements of flow and concentrations at the same point, the tip of the O_2 sensor in these instruments is positioned

55   at a few centimeters horizontal distance from the ADV's measuring volume to prevent disturbances of the flow and acoustic ADV signal through reflections off the O_2 sensor. The ensuing time-shift between flow and associated oxygen data can produce errors in the flux calculations, and algorithms were developed that shift the O_2 data in time such that they are synchronized with the velocity data (McGinnis et al., 2008a;Berg et al., 2015;Reimers et al., 2016). In steady unidirectional flow, this procedure largely can eliminate time-shifts, but it is difficult to apply an effective correction in highly dynamic environments

60   with rapid changes in magnitude and direction of flow as the reef ecosystem (Donis et al., 2015;Reimers et al., 2016). While such a correction theoretically is possible using the three-dimensional velocity data, the cumulative effect of innate small uncertainties in such calculations can lead to large under-or overestimates of the flux (Berg et al., 2015;Reimers et al., 2016). To determine the benthic O_2-flux of carbonate sands in energetic reef environments, we therefore designed a triple O_2-sensor eddy covariance instrument (3OEC) that eliminates the error caused by the spatial separation of flow and concentration

65   measurements. The deployments took place in the Florida Keys at an exposed inner shelf site with highly permeable sands,

very clear oligotrophic water and substantial wave action. Comparison with an eddy covariance instrument with conventional sensor configuration was used to analyze magnitudes of potential flux errors and the effectiveness of standard data corrections.

2 Methods

2.1 Triple O_2-sensor eddy covariance instrument (3OEC)

70 The 3OEC uses simultaneous measurements of three O_2-fiber optodes. These optodes are positioned with 120 degrees angular spacing in the same horizontal plane around the centre point of the water volume where current flow is measured by the ADV (Fig. 1). Since the natural flow field is nearly homogeneous at the length scale of the sensor spacing (6.4 cm between O_2-sensors), an O_2 concentration closely corresponding to that at the flow measuring point can be calculated through averaging of the three optode signals, which largely eliminates errors caused by the spatial separation of oxygen and flow measurements.
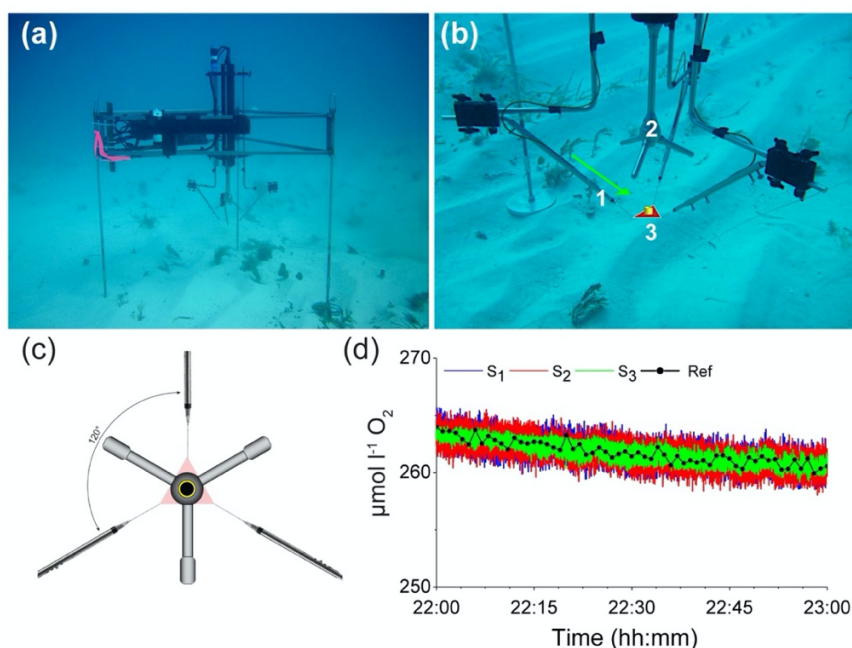
Figure 1: The triple O_2-sensor eddy covariance instrument (3OEC). (a) The 3OEC deployed over carbonate sand at the study site in the Florida Keys. (b) Positioning of the ADV sensor head (centre) and the three O_2-sensors. The average O_2 concentration calculated from the signals of sensors 1, 2 and 3 approximates the concentration at the geometric centre of the red triangle (side lengths 6.4 cm) defined by the three O_2-sensor tips, which is located within the flow measuring volume of the ADV (yellow cylinder). The green arrow indicates the main flow direction. (c) Vertical view of the positioning of the O_2 sensors around the ADV measuring volume (yellow circle) that is located 15 cm below the central sensor stem. The sensor tips were located at 3.0 cm horizontal distance from the lower edge of the ADV measuring volume. Red triangle is the vertical view of the red triangle shown in (b). (d) Example on a one-hour interval of the O_2-readings of the three fibre optodes (green, red, blue lines) and the reference planar optode (black line and dots) recorded during the deployment on July 16, 2017.

75 The optodes are ultra-highspeed O_2-needle sensors (Pyroscience™- OXR430-UHS, Table A1) with a response time of 200-300 ms (Merikhi et al., 2018). The three optodes are pointing downward at a 45° angle, with their sensing tips positioned at 3.7 cm horizontal distance from the centre of the flow measuring volume. This placement, within the recommended distance of 10 Kolmogorov scale lengths from the ADV measuring volume (Lorrai et al., 2010), prevents any disturbance of the flow in that volume and potential interferences with the acoustic pulses of the ADV. The sensors are read by three FireStingO2-

80 Mini O_2-meters (Pyroscience™, Table A2). The ADV is a Nortek™ Vector acoustic Doppler velocimeter (Table A3) that measures the 3D velocity field within a cylindrical measuring volume (1.5 cm diam. x 1.5 cm, located 15 cm below the central acoustic transducer) at a sampling rate of 32 Hz. A DataQ DI-710-UH USB data logger (14-bit A/D conversion) records simultaneously the output of O_2-meters and the ADV at a rate of 64 Hz to prevent aliasing. O_2-meters and data logger are contained in an underwater housing (A.G.O Environmental Electronics) fitted with three Pyroscience™ fibre feed through

85 plugs for connecting the O_2-sensors, and Impulse micro inline plugs for connecting the ADV and external battery (4 x Lithium-Ion 12 V, 50 Wh). The ADV, O_2 meter housing, and battery pack are mounted on a stainless-steel tripod with 1.2 m side length and 1.2 m height (Berg and Huettel, 2008). In addition, the frame carries a MiniDot O_2-logger (PME) and an Odyssey PAR-logger (Dataflow Systems) for collection of temperature and O_2 reference data (once per minute) and photosynthetically active radiation (PAR) data (once per 10 minutes), respectively.

2.2 Dual O_2-sensor eddy instrument (2OEC)

90

A 2OEC with conventional sensor configuration was deployed parallel to the 3OEC to analyse the potential flux error caused by the time-shift and the effectiveness of standard data corrections. The 2OEC, described in detail in Huettel et al. (2020), measures simultaneously with two O_2-optodes positioned on one side of the ADV measuring volume with their measuring tips 1 cm horizontally apart. Deployments of this instrument at the same study site in the Florida Keys simultaneously with benthic

95 advection chambers (Huettel and Gust, 1992;Janssen et al., 2005;Huettel et al., 2020) produced eddy covariance fluxes (3.7 ± 0.9 mmol m^{-2} h^{-1}) that were very similar to those of the chamber fluxes (3.9 ± 3.0 mmol m^{-2} h^{-1}) during daytime, and of similar order of magnitude during nighttime (2OEC: -2.5 ± 1.3 mmol m^{-2} h^{-1}, chambers: -3.4 ± 0.8 mmol m^{-2} h^{-1}). These fluxes obtained with an independent measuring technique corroborate the magnitude of the eddy covariance fluxes, but it should be noted that the chambers do not account for changes in flow and organic matter supply during the incubation, which both have significant

100 influence on flux. While the chambers under relatively steady conditions can produce fluxes similar to those recorded by eddy covariance instruments, discrepancies between fluxes measured by the two techniques were observed in dynamic environments (Berg et al., 2013).

2.3 Data processing

Eddy covariance flux calculations are based on the assumption that the flux signal is transported by a bottom current with

105 steady state mean flow and O_2 concentration that reaches the instrument unobstructed after passing the footprint area (Massman

and Lee, 2002;Baldocchi, 2003;Kuwae et al., 2006;Berg et al., 2007). In coastal environments, such conditions rarely are met, requiring post processing of the flux data to correct for infringements of these assumptions as well as errors caused by technical limitations (Holtappels et al., 2013;Reimers et al., 2016;Huettel et al., 2020). We applied the same routine corrections to 3OEC and 2OEC data for compensation of design and sensor limitations as well as for non-steady-state O_2 concentrations in the water

110   column. The unfiltered flow and O_2 data were reduced from 64 Hz to 8 Hz by averaging, which reduced noise but maintained sufficient resolution to describe the entire frequency spectrum carrying the flux signal. For each 8 Hz time point, the average signal of the three O_2-sensors of the 3OEC were calculated to determine an estimate of the O_2 concentration in the centre of the ADV measuring volume. Similarly, the signals of the two sensors of the 2OEC were averaged to produce mean concentrations. O_2 fluxes then were calculated based on these averages as well as on the signals of each individual sensor using

115   the software EddyFlux 3.2 (Berg unpublished). The software determines mean O_2 base concentrations for 15 min time segments through Reynolds decomposition (Lorrai et al., 2010;Berg et al., 2009;Lee et al., 2004). Within each 15-minute interval, the mean O_2 concentration $\overline{O_2}$ (defined as a least-square linear fit to the data) then is subtracted from each 8 Hz O_2 data point to arrive at the instantaneous O_2 fluctuation O_2' for that time point. The instantaneous vertical velocity V_z' is determined using the same procedure. The flux at each 8 Hz time point is calculated by multiplying the instantaneous vertical

120   velocity and associated instantaneous O_2 concentrations. These fluxes were averaged over the 15-minute time intervals. To determine day(light)- and night(dark) fluxes, the changes in the 15-minute fluxes were added over time to produce cumulative flux curves. For three consecutive time intervals (42 to 95 minutes in length) with undisturbed flux during day and night, slopes of these curves then were calculated to determine light- and dark fluxes, respectively. In the following text, fluxes based on the averaged signal of 3 or 2 O_2 sensors was termed "3S-flux" and "2S-flux" respectively. Single sensor fluxes were termed

125   "1S-flux" and uncorrected fluxes "raw" fluxes.

Standard corrections, abbreviated in this text by single letters, were applied to the flux data to reduce errors caused by instrument tilt (R), wave effects (W), time-shift (T) caused by spatial separation of sensors (2OEC) and sensor response time, and changes in water column O_2 storage (S) (Berg et al., 2015;McGinnis et al., 2008a;Lorke et al., 2013;Huettel et al., 2020).

130   Influence of potential instrument tilt (R) on flux was tested and corrected when necessary, through rotation of the velocity data so that the mean transverse and vertical velocity was nullified (Lee et al., 2004;Lorke et al., 2013;Lorrai et al., 2010). Similarly, wave rotation (W) was rectified by rotating the flow velocity field so that $SD(V_y)$ and $SD(V_z)$ reached a minimum (SD represents 1 standard deviation)(Berg et al., 2015;Berg et al., 2013). Time-shifts (T) were rectified through applying time-shift corrections to the O_2 data that produced the maximum absolute fluxes (McGinnis et al., 2008a;Berg et al., 2015;Berg et al.,

135   2003;Reimers et al., 2016;Fan et al., 1990). Effects of large-scale variations in the average water column O_2 concentration (S) were compensated through applying an O_2 storage term ($J_{St} = \int_0^h dC/dt\, h$, with dC/dt : change of the average O_2 concentration over time, calculated through linear detrending of the measured O_2 data over 15 minute intervals, h : height of the measuring volume) (Holtappels et al., 2013;Rheuban et al., 2014). Furthermore, acceleration or deceleration of current flows can alter the O_2 concentration profile and thereby temporarily modulate vertical flux (Holtappels et al., 2013). Our data analysis indicated

5

140   that the temporal flux variations caused by transient velocity changes largely cancelled out over time, and a correction for transient velocity changes was not applied.

Daytime was defined as the period between sunrise and sunset. To determine the significance of differences between fluxes, the t-test was utilized. Error margins are reported as ± 1 standard deviation unless stated otherwise.

145   **2.4 Instrument deployments**

The 3OEC and 2OEC were deployed at 9 ± 1 m water depth on an exposed backreef carbonate platform in the Florida Keys (24° 43.523'N, 80° 49.855'W, Fig. 2) on July 11, 13, 15, and 16, 2017. The seafloor here is covered by highly permeable medium carbonate sand (median grain size: 440 μm, permeability: $3.2 \times 10^{-11} \pm 1.2 \times 10^{-12}$ m^2) with relatively low carbon content (0.23% ± 0.05% sed. dw.) and colonized by microphytobenthos (Chlorophyll a: 4.9 ± 0.1 μg g^{-1} sed. dw.). SCUBA-divers

150   placed the two instruments 10 m apart, along a transect perpendicular to the main southwest-northeast flow direction. The tripods were rotated such that the X-axis of the ADVs was aligned with the main current direction, and the measuring volumes of the ADVs were adjusted to 35 cm above the seafloor. During the deployment week, water temperatures averaged 29.9 ± 0.3 °C and salinity 35.0 ± 0.5. Bottom current velocities ranged from 5 to 14 cm s^{-1}. Waves increased from 11 July to 15 of July, when maximum wave heights of 90 cm were reached, and then dropped again on 16 July. The weather was mostly sunny with

155   some scattered clouds resulting in relatively high light intensities at the seafloor reaching 392 μmol photons m^{-2} s^{-1}. On each measuring day, the instruments were deployed during daylight time to include the effect of benthic photosynthesis and were retrieved the following day for data download.

3 Results

3.1 Benthic fluxes

160   Daytime 3OEC O$_2$-fluxes averaged 5.2 ± 0.6(SE) mmol m^{-2} h^{-1}, nighttime fluxes -2.8 ± 0.6(SE) mmol m^{-2} h^{-1}, characterizing the permeable carbonate sand bed as a site of high carbon turnover and net autotrophy in July 2017 (Fig. 2). Average 2OEC daytime fluxes were 7% higher and nighttime fluxes 27% higher than the respective 3OEC fluxes but both differences were statistically not significant (daytime: t(DF 6) = 0.3621, p (two-tail, 95%) = 0.7297, nighttime: t(DF 6) = -0.9721, p (two-tail, 95%) = 0.3686).

165
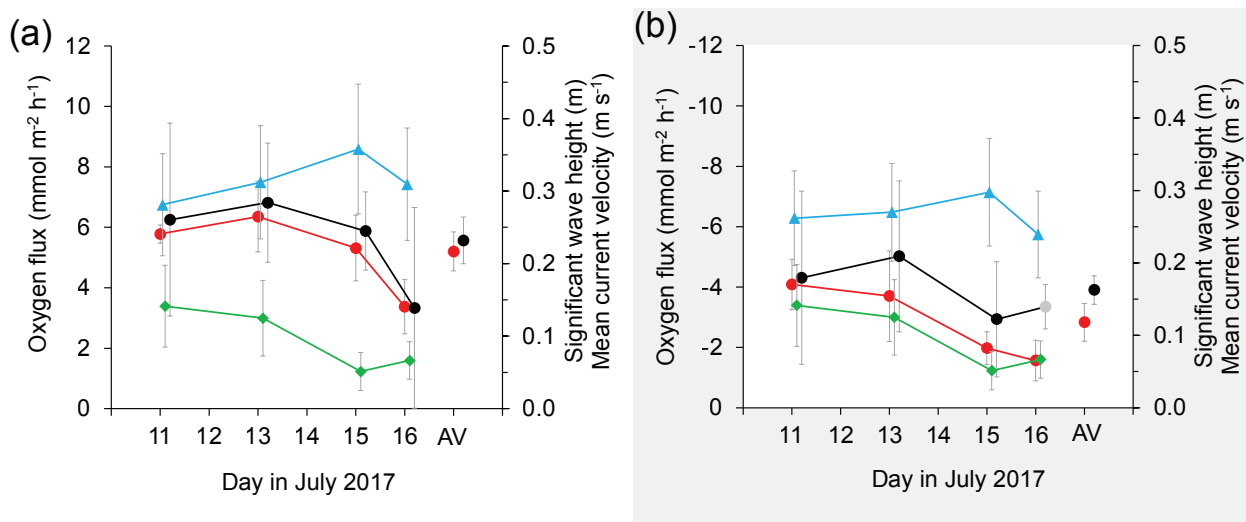
Figure 2: Fluxes, waves and currents measured during the deployment week. 3OEC (red circles and line) and 2OEC (black circles and line) -measured O₂ fluxes, significant wave height (light blue triangles and line) and current flow (green diamonds and line) during (a) day and (b) night recorded in July 2017. Note reversed Y axis scale for (b) night fluxes. Grey circle in (b) indicates data point compromised by sensor deterioration. Error bars depict standard deviation, except for the 11-16 July averages (single circles on right side of panes), where error bars present standard error.

These trends scaled with bottom flow velocity that slowed during the deployment week (~30 mmol m^{-2} h^{-1} flux increase or decrease per m s^{-1} flow decrease, Fig. 3a). In contrast, significant wave height increased during the study except the last day.

170

Light conditions were similar between deployment days (858 ±165 mmol photon m^{-2} surface PAR for the overlapping time period 17:00-20:00) and the community photosynthesis-irradiance (PI) curves (Bernardi et al., 2015) predicted maximum gross benthic primary production (GPP) of 9.9 (3OEC) and 10.7 mmol O$_2$ m^{-2} h^{-1} (2OEC) (Fig. 3b). Light utilization efficiency (LUE, ratio between GPP and PAR) ranged between 0.07-0.08 O$_2$ photon^{-1} at 350 μmol photon m^{-2} s^{-1} to 0.09-0.10 O$_2$ photon^{-1}

175 at 10 μmol photon m^{-2} s^{-1} (Fig. 3c).
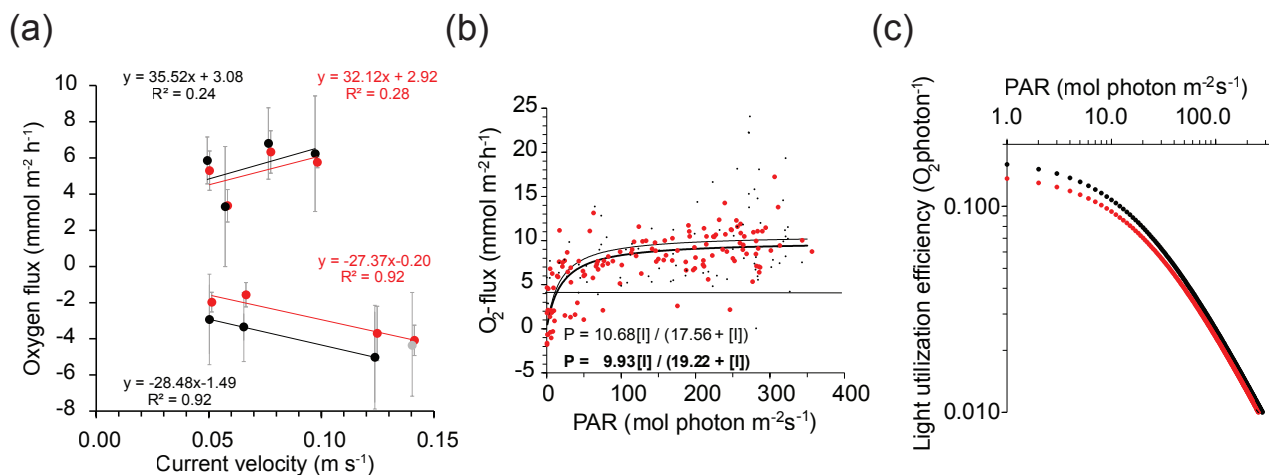
Figure 3: Effect of flow and light on flux. (a) Effect of flow velocity on day- and nighttime fluxes measured with the 3OEC (red circles and line) and 2OEC 4 (black circles and line). Compromised data point from the 16 July 2OEC deployment excluded from regression (grey circle). (b) Increase of daytime fluxes with increasing light intensity at the seafloor. Black curves depict photosynthesis-irradiance-curves (red circles, thick line: 3OEC, black dots, thin line: 2OEC) calculated using Michaelis-Menten kinetics ($P = P_{max} [I] / (K_I + [I])$), with P: photosynthetic rate at a given light intensity, P_{max}: maximum potential photosynthetic rate, [I]: light intensity, K_I: half-saturation constant, i.e., the light intensity at which the photosynthetic rate proceeds at ½ P_{max}). Horizontal black line indicates approximate level of daytime respiration. (c) Light utilization efficiency of the benthic community based on data shown in (b) (red circles: 3OEC, black circles: 2OEC).

3.2 Comparison of 3OEC and 2OEC fluxes

180   Magnitudes and dynamics of the O_2 fluxes recorded by the 3OEC and 2OEC were similar (Fig. 4). In both instruments, the fluxes based on the individual O_2 sensor signals in general agreed. Averaging of the sensor signals in the 3OEC reduced the error margin of the flux estimates by 27% ± 35%(1SD) during daytime and 114% ± 158%(1SD) during nighttime (Fig. 5a). The normalized daytime 3OEC 1S-fluxes deviated 3.4% ± 2.6% (1SD), nighttime fluxes 18.4 % ± 15.7%(1SD) from the respective normalized 3S-fluxes (Fig. 5b). The same trend was observed in the 2OEC data, here the normalized 1S fluxes

185   deviated from the normalized 2S flux by 2.2% during daytime and 26% during nighttime (Fig. 5b). Corrections for storage (S) and time-shift (T) increased the raw flux, while corrections for wave rotation (W) and instrument tilt (R) reduced it (Fig. 5c). Applying a combination of storage, time-shift and wave rotation corrections (STW) led to the best agreement between 1S fluxes as well as to the strongest enhancement of the raw flux (Fig. 5 c,d), as previously found in 2OEC deployments conducted at the same study site (Huettel et al., 2020).

190
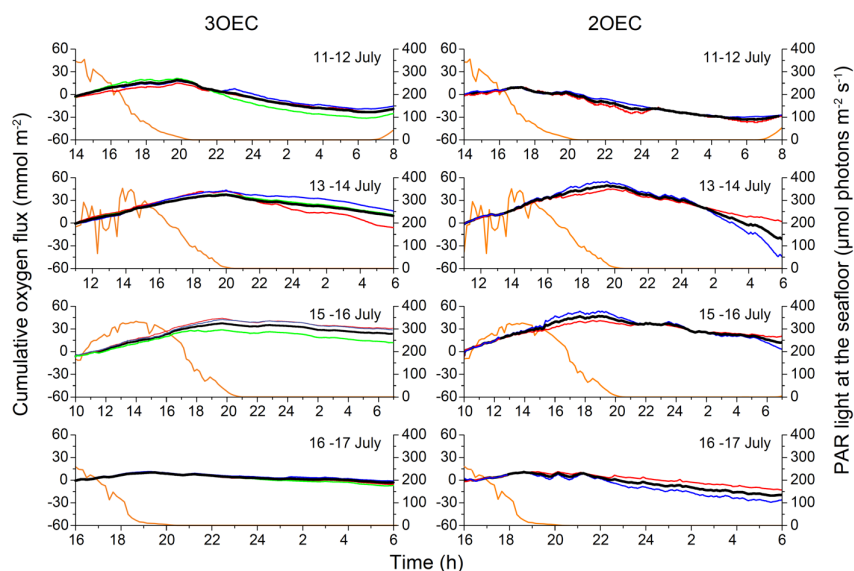
Figure 4: Comparison of 3OEC and 2OEC fluxes. Cumulative fluxes for July 11-12, 13-14, 15-16 and 16-17 (top to bottom) with the respective light (PAR) intensities (orange lines) at the seafloor for 3OEC (left column) and 2OEC (right column). Sensor 1: red, Sensor 2: blue, Sensor 3: green, average sensor signals: black thick lines.
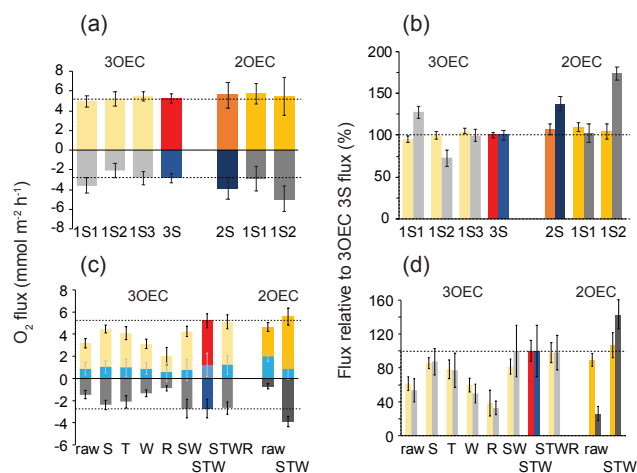

Figure 5: Comparison of fluxes based on single sensor signals and average signals, and the effects of flux corrections. (a) Comparison of the daytime (yellow/orange) and nighttime (grey/dark grey) fluxes averaged over all days based on individual sensors and sensor averages (day: red/brown, night: blue/darkblue). 2OEC data presented in the darker color shades (b) normalized 1S, 2S and 3S fluxes, color code as in (a). The 3S flux (red/blue) was set to 100% (all data in (a) and (b) are STW- corrected, error bars are SE). (c) Effect of corrections on 3S and 2S daytime, nighttime and 24h fluxes (light blue) averaged over all days (error bars SE). raw: not corrected, S: Storage-corrected, T: Time-shift-corrected, W: Wave rotation-corrected, R: Rotation-corrected, SW, STW, STWR are combinations of the above corrections. (d) normalized differences between the 3OEC STW-corrected average fluxes (set to 100%) and fluxes with no correction or different corrections recorded with the 3OEC and the 2OEC (error bars SE). Column color coding in (c) and (d) as listed for (a). Dotted lines allow comparison of the fluxes with the 3S fluxes. Corresponding graphs based on the individual sensor readings are available in the supplemental materials.

4 Discussion

The O2-fluxes recorded by the 3OEC characterized the coarse carbonate reef sands as sites of intense benthic production and
195 respiration (Fig. 6). The nighttime O2 consumption rates of the coral sand ranged among the highest respiration rates reported
for shallow shelf sediments, matching or exceeding rates measured in other coral reef sands (Cyronak et al., 2013;Eyre et al.,
2013;Grenz et al., 2003;Rasheed et al., 2004;Wild et al., 2005a;Wild et al., 2004a).
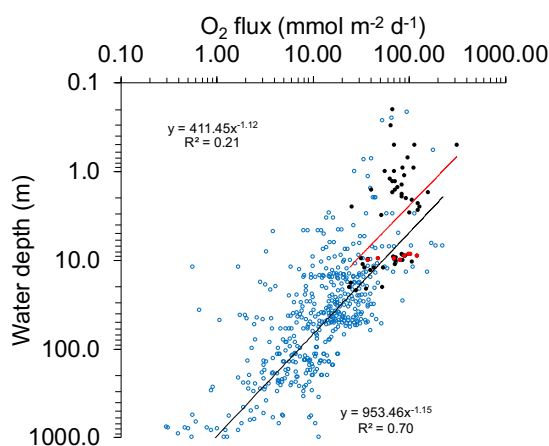
**Figure 6: Comparison of fluxes measured in this study with benthic O2 consumption rates in the continental shelf and
adjacent slope sediments reported in the literature. Red circles: O2 consumption rates measured in this study. Black
circles: O2 consumption rates of carbonate reef sands from (Santos et al., 2011;Glud et al., 2008;Boucher et al.,
1994;Grenz et al., 2010;Cyronak et al., 2013;Eyre et al., 2013;Grenz et al., 2003;Rasheed et al., 2004;Wild et al.,
2005a;Wild et al., 2005b;Wild et al., 2004a;Wild et al., 2004b;Wild et al., 2004c). Open blue circles: Benthic O2
consumption rates for sediments at different water depth ((Glud, 2008;Middelburg et al., 2005;Hopkinson and Smith,
2005;Laursen and Seitzinger, 2002) and studies compiled in these reviews). Red line: exponential fit of the decrease of
carbonate sand respiration (black and red circles) with depth (decay coefficient -1.12 mmol m-2 d-1 m-1). Black line:
exponential fit of the decrease of silicate sediment (blue open circles) respiration with depth (decay coefficient -1.15
mmol m-2 d-1 m-1)**

200 Since the coral sands at our site are low in organic carbon (< 0.3% dw) and occur in an oligotrophic subtropical reef
environment with low water column chlorophyll and dissolved organic carbon content (NO3+NO2 < 0.2 µmol l⁻¹, NH4 < 0.5
µmol l⁻¹, PO4 < 0.05 µmol l⁻¹, Chl. a < 0.2 µg l⁻¹, DOC < 200 µmol l⁻¹, Huettel unpublished) a substantial sedimentary source
of reduced compounds is required to maintain these high respiration rates. The compensation light intensity (intensity at which
O2 production exceeds respiration) reached at ~12 µmol photons m-2 s-1 and the high light utilization efficiency of 0.09-0.10
205 O2 photon-1 near the theoretical limit (0.12 O2 photon-1, (Brodersen et al., 2014)) revealed that the microphytobenthos could
maintain excess production under cloudy conditions, identifying the sedimentary microalgae as source for the intense organic

matter production and export. The estimated maximum production of ~10 mmol m^{-2} h^{-1} in the Florida carbonate sands (Fig. 3b), is in line with rates reported for reef lagoon sediments in Moorea (P_{max} 6.8 ± 0.5 mmol m^{-2} h^{-1} (Boucher et al., 1998)), New Caledonia (P_{max} ~10 mmol m^{-2} h^{-1} (Clavier and Garrigue, 1999)) and the Great Barrier Reef (P_{max} ~11 mmol m^{-2} h^{-1} (Eyre

210   et al., 2013)). To put these rates into perspective, eddy covariance flux measurements over dense Mediterranean *Posidonia* seagrass meadows (13 m depth, PAR 300-400 μmol photons m^{-2} s^{-1}) produced daytime O_2-fluxes of 6.8 ± 0.7 μmol m^{-2} h^{-1} and nighttime fluxes -3.6 ± 0.4 μmol m^{-2} h^{-1} (Koopmans et al., 2020), i.e. rates of the same magnitude as measured in the microphytobenthos communities. The trends of nighttime respiration that mirrored those of daytime production (Figs. 2, 4) indicate that at our site microphytobenthos drove the high O_2 consumption rates through its respiration and by producing highly

215   degradable organic matter that was promptly recycled by the benthic heterotrophic community. Factors contributing to the high microbial activity in the carbonate sands include the high specific surface area of the biogenic grains, their permeability to water and gases, the organic content of the grains, their chemical buffering capacity, and their light guiding characteristics (Marcelino et al., 2013;Huettel et al., 2014;Wild et al., 2006;Wild et al., 2005a).

220   Another influential factor modulating the microbial activity in the permeable carbonate sands were the bottom currents and the advective pore water exchange they produced (Huettel et al., 2014). Waves were relatively high for this shallow environment and wave orbital motion influenced water movement and pressure near the seafloor during the entire study (Fig. 8). Yet, fluxes scaled with the average unidirectional bottom current (Fig. 2) that decreased over the study period and not with significant wave height, which increased except on the last deployment day. On that last day, significant wave heights were

225   nearly identical to those recorded three days earlier during the 13-14 July deployment (Fig. 2, day: 0.31, 0.31 m, night: 0.27, 0.24 m, for 13-14 and 16-17 July, respectively), nevertheless daytime fluxes decreased by 47% and sand nighttime fluxes by 58% between these deployments. Given that the light conditions at the seafloor did not change significantly during the study week, this indicates that the horizontal bottom current dominated benthic flux modulation, while wave orbital motion had less of an impact. The consistent positive influence of current flow on flux (Fig. 3a) supports this evaluation and agrees with results

230   of earlier studies that found an enhancing effect of current on flux for environments with permeable sediment (Berg et al., 2013;Chipman et al., 2016;McGinnis et al., 2014). Continuous flow may be more effective than oscillating flow in driving advective pore water exchange in permeable sediments. In contrast to the steady pressure gradients continuous flows generate, wave orbital motion produces oscillating gradients, which enhance turbulence in the pore space of the sand (Horton and Pokrajac, 2009;Jouybari et al., 2020). This turbulence and inertial losses associated with the acceleration and deceleration of

235   the pore flows may lessen the effects of pressure gradients driving the advective pore flows and interfacial water exchange. The frequency spectrum of the turbulence in the bottom flows influences how the flux signal is transported in the water column. Waves can produce artefacts in measured fluxes (Berg et al., 2015), which may have been largely eliminated by the measuring heights we used. In a recent study, Long (2021) proposed positioning the eddy covariance measurement point higher in the water column to reduce flux bias caused by waves. Long's study site with carbonate sands at 6 m water depth off Key Largo

240   (Florida) was close (68.5 km distance) and very similar to ours, and his measuring height (35 cm) was identical to the one we

used. The fluxes Long measured in June 2018 reached 5 mmol O_2 m^{-2} h^{-1} during daytime and -3 mmol O_2 m^{-2} h^{-1} during nighttime, similar to the fluxes we measured (5.2, -2.8 mmol O_2 m^{-2} h^{-1}).

Co-spectra time series, plotted for hourly intervals from 16:00 to 24:00 for our 4 deployments indicate that during the transition
245 from light to dark (Fig. 7, 16:00-19:00, warm colours), turbulence within a frequency < 0.1 Hz still had a positive flux signal, while the higher frequency turbulence already carried a negative signal. As the microphytobenthos photosynthetic O_2 production declined with the decreasing light intensity at the seafloor, flux switched from benthic O_2-release to O_2-uptake. The ensuing negative benthic flux signal initially was transported by the fast small eddies generated at the rough sediment-water interface, while the slower large eddies higher in the water column still carried the positive flux signal. The co-spectra
250 document the gradual mixing of the smaller eddies with negative flux signal into the large eddies with positive flux signal, i.e., the negative flux dip in the daytime co-spectra broadened with decreasing light conditions, expanding from the higher to lower frequencies. This eddy memory effect decreased with the general decrease of bottom current velocity during our field campaign, as less high frequency, small eddy turbulence is created at the sediment water interface at lower flow velocities (Lee and Cheung, 1999;Sleath, 1974). Consequently, the negative dip in the daytime co-spectra disappeared and the co-spectra
255 appeared almost undisturbed in the last deployment (16-17 July).
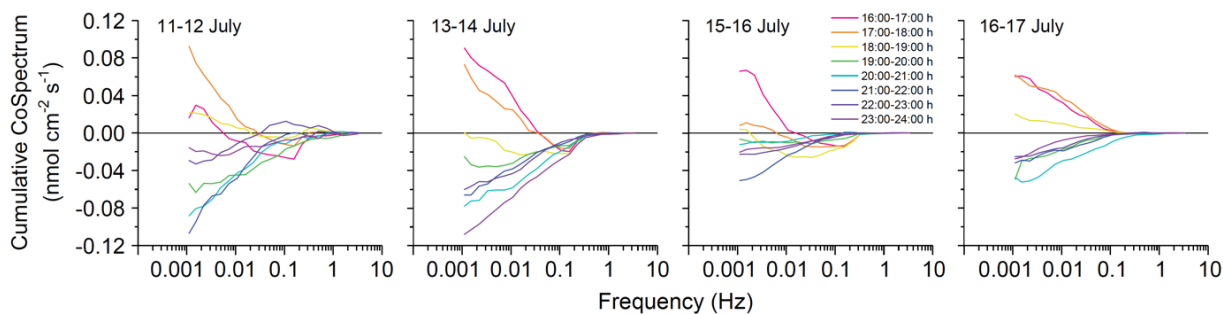
Figure 7. Change of the cumulative co-spectra for the 3S O_2 flux during the deployment week. Cumulative co-spectra were calculated for hourly intervals from 16:00 to 24:00 for the four deployment periods (0.12 nmol cm^{-2} s^{-1} corresponds to 4.3 mmol m^{-2} h^{-1}). Colors indicate the time periods for which the co-spectra were calculated.

The overall good agreement between the 3OEC and 2OEC strengthens the calculated fluxes. Averaging of the three optode signals reduced the error margins of the 3OEC fluxes relative to the 2OEC fluxes (Figs. 2, 5) through elimination of the time-shift caused by spatial separation of O_2 and flow measurements. Nevertheless, a time-shift remains, which is caused by the
260 response time of the O_2 sensors (0.2-0.3 s) and temporary distortions of the O_2-concentration field. In the 4-minute recording section shown in Figure 8, the wobbling in the vertical connecting lines between the O_2-concentration minima recorded by the three optodes reveals such distortions at the scale of the oxygen sensor spacing (i.e., within the red triangle in Fig. 1). Nearly parallel connecting lines during time intervals with reduced wave activity (e.g., 40-60 s, 90-120 s, 210-220 s) confirmed that the sensor response times were similar and consistent, while the positive as well as negative time offsets observed between the

265   maxima of elevation (i.e., the instantaneous relative position of a water parcel (Berg et al., 2015)) and the associated O$_2$-signal

minima implied that the wobbling was not related to optode response characteristics. Distortions in the concentration field
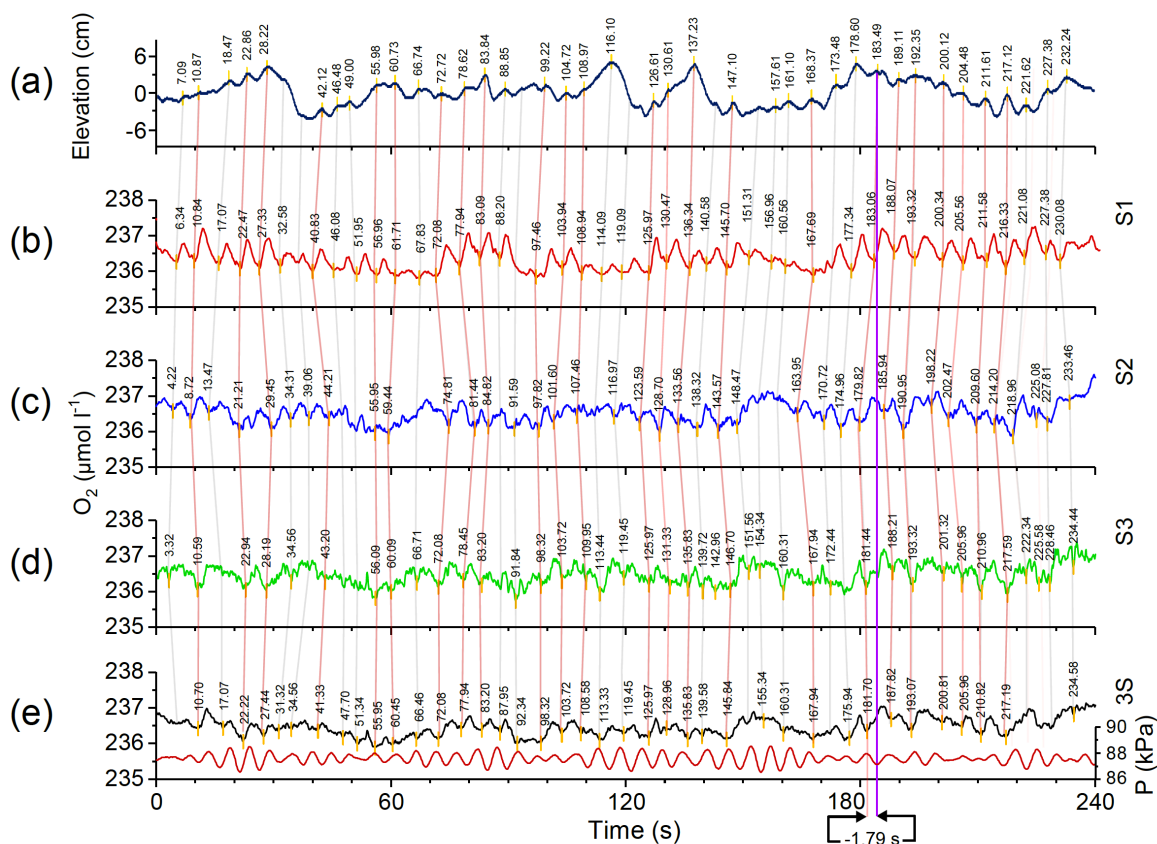
Sensor or AV	O$_2$ max.	O$_2$ min.	O$_2$ range	O$_2$ AV	O$_2$ SD	O$_2$ Variance	max. pos. time-shift	max. neg. time-shift	average time-shift	time-shift variance
	(µmol l^{-1})					(µmol l^{-1})^2	(s)			(s^2)
S1	238.61	235.02	3.60	236.38	0.71	0.51	1.08	-1.76	-0.36	0.59
S2	238.12	235.03	3.09	236.53	0.53	0.28	2.82	-4.42	-1.52	3.92
S3	239.76	234.13	5.63	236.48	0.70	0.48	1.48	-2.05	-0.20	0.82
3S	**238.22**	**235.31**	**2.92**	**236.46**	**0.39**	**0.15**	**1.48**	**-1.79**	**-0.59**	**0.58**

Figure 8. Four-minute interval of nighttime data recorded on July 13th (4:53:20-4:57:20) comparing the simultaneous elevation, oxygen and pressure readings recorded by the 3OEC. (a) elevation (blue line) and (b, c, d) the associated O$_2$ concentrations recorded by the three optodes (red, blue and green lines) and their (e) average (black line). Brown line in (e) depicts pressure P (scale right Y axis) at the height of the ADV. The data were smoothed by a 2.5 s running average. In absence of a time-shift, a minimum in O$_2$ change occurs when water displacement is zero, and points with zero O$_2$ change therefore are connected in this graph to points with no elevation change. Since this is a nighttime recording, O$_2$ minima cross-correlate with elevation maxima. Vertical red lines connect elevation maxima and associated O$_2$ minima as identified by the Origin lab 2017 software peak-finding algorithm (analysis of 2nd derivative). Grey vertical lines do the same but in these cases one of the minima or maxima could not be identified by the peak-finding algorithm. The instance of the largest temporary time-shift (-1.79 s) between elevation maximum and the corresponding 3S-O$_2$-minimum observed within this 4 min interval is indicated by the vertical purple line. The data listed below the graph reveal how the averaging of the O$_2$ signals reduces the variance of the O$_2$ signal in the flow measuring volume relative to the individual O$_2$ signals.

13

move the 3S signal slightly off centre in the flow measuring volume, temporarily producing time-shifts between 3S signal and velocity data. In this example, a maximum time-shift of 1.79 s briefly was reached at t = 183.49 s, lasting less than 6 s. The

270 total time-shift caused by sensor response time plus these transitory shifts during these 4 minutes averaged -0.36, -1.52 and -0.20 s for the three sensors, respectively, and -0.59 s for the 3S signal. To compensate for sensor response time, a time-shift correction was included in the corrections (STW) used when calculating all 3S fluxes. The temporary time-shifts caused by transitory concentration field distortions average out over time as reflected in the 3S variances that were 1.9 to 3.4-times smaller than the 1S variances, and a correction for concentration field distortion was not applied.

5 Conclusions

O_2-flux is a key indicator for changes in benthic metabolism and ecosystem health, emphasizing the need for reliable flux estimates. The aquatic eddy covariance technique arguably is the best available method for measuring flux at the seafloor as it does not alter activities of benthic fauna and flora, integrates effects of patchiness, and accounts for the effects flow, light, temperature as well as the supply of electron donors and acceptors that control the fluxes. In energetic environment with waves,

280 time-shift corrections can lead to substantial flux errors (Berg et al., 2015;Reimers et al., 2016), and the elimination of the time-shift caused by spatial separation in the 3OEC can effectively reduce errors in such settings. The 3OEC presents a hardware solution designed to measure fluxes in dynamic benthic environments, and we consider the O_2-fluxes produced by this instrument as some of the most realistic flux estimates achievable with present day technology. The 3OEC data reported here reveal the high O_2 production and consumption in highly permeable carbonate coral reef sands, emphasizing the central

285 role of microphytobenthos for the carbon cycling in these oligotrophic environments.

6 Appendix A

290 **Table A1: Specifications of the Pyroscience™ OXR430-UHS retractable oxygen minisensors**

Optical O_2 fiber sensor type	Pyroscience™ OXR430-UHS
Fiber diameter	430 μm
Optimal measuring range	0-720 μmol l^{-1}
Maximum measuring range	0 - 1440 μmol l^{-1}
Detection limit	0.3 μmol l^{-1}
Resolution at 1% O_2	0.16 μmol l^{-1}
Resolution at 20% O_2	0.78 μmol l^{-1}
Accuracy at 1% O_2	± 0.31 μmol l^{-1}
Accuracy at 20% O_2	± 3.13 μmol l^{-1}
Temperature range	0 - 50°C

Table A2: Specifications of the Pyroscience™ FireStingO$_2$-Mini oxygen meter

Pyroscience™ FireStingO$_2$-Mini	Single sensor module,
Oxygen port	1 fiber-optic ST-connector
Temperature port	4-wire PT100, -30°C-150°C, 0.02°C resolution, ±0.5°C accuracy
Dimensions and Weight	67 x 25 x 25 mm, 70 g
Measuring principle	Luminescence lifetime detection (REDFLASH)
Excitation Wavelength	620 nm (orange-red)
Emission wavelength	760 nm (NIR)
Maximum sampling rate	20 Hz
Interface	Serial interface (UART), ASCII communication protocol
Analog output	0 - 2.5 V DC, 14 bit resolution
Power requirements	Max. 70 mA at 5 V DC from USB (typ. 50 mA)

Table A3: Specifications of the NORTEK Vector acoustic Doppler velocimeter

Sensor	Range	Accuracy	Precision/Resolution
Velocity	±0.01, 0.1, 0.3, 1, 2, 4, 7 m s^{-1}	± 0.5%	± 1%
Pressure	0-20 m (shallow water version)	0.5% (full scale)	< 0.005% of full scale
Temperature	-4 to +40 °C	0.1 °C	0.01 °C
Compass	360º	2º	0.1º
Tilt	< 30°	0.2°	0.1°

295

7 Data availability

Current flow, pressure, and oxygen concentrations recorded by the 3OEC-instrument (doi:10.26008/1912/bco-dmo.849934.1), reference temperature and dissolved oxygen (doi:10.26008/1912/bco-dmo.849915.1) and PAR data

300 (doi:10.26008/1912/bco-dmo.849979.1) recorded 11-17 July 2017 are available at the Biological and Chemical Oceanography Data Management Office (BCO-DMO, https://www.bco-dmo.org/).

8 Author contributions

AM deployed the 3OEC, analysed the data, and wrote the first version of the manuscript. MH designed and built the 3OEC instrument. MH and PB contributed to the data analysis and the preparation of the manuscript.

305 ## 9 Competing interest statement

The authors declare that they have no conflict of interest.

10 Acknowledgments

References

Albright, R., Takeshita, Y., Koweek, D. A., Ninokawa, A., Wolfe, K., Rivlin, T., Nebuchina, Y., Young, J., and Caldeira, K.: Carbon dioxide addition to coral reef waters suppresses net community calcification, Nature, 555, 516-+,
315 10.1038/nature25968, 2018.

Attard, K. M., Hancke, K., Sejr, M. K., and Glud, R. N.: Benthic primary production and mineralization in a High Arctic fjord: in situ assessments by aquatic eddy covariance, Marine Ecology Progress Series, 554, 35-50, 10.3354/meps11780, 2016.

Baldocchi, D. D.: Assessing the eddy covariance technique for evaluating carbon dioxide exchange rates of ecosystems: past, present and future, Global Change Biology, 9, 479-492, 10.1046/j.1365-2486.2003.00629.x, 2003.

320 Berg, P., Roy, H., Janssen, F., Meyer, V., Jorgensen, B. B., Huettel, M., and de Beer, D.: Oxygen uptake by aquatic sediments measured with a novel non-invasive eddy-correlation technique, Marine Ecology-Progress Series, 261, 75-83, 2003.

Berg, P., Roy, H., and Wiberg, P. L.: Eddy correlation flux measurements: The sediment surface area that contributes to the flux, Limnology and Oceanography, 52, 1672-1684, 2007.

Berg, P., and Huettel, M.: Monitoring the Seafloor Using the Noninvasive Eddy Correlation Technique: Integrated Benthic
325   Exchange Dynamics, Oceanography, 21, 164-167, 2008.

Berg, P., Glud, R. N., Hume, A., Stahl, H., Oguri, K., Meyer, V., and Kitazato, H.: Eddy correlation measurements of oxygen uptake in deep ocean sediments, Limnology and Oceanography-Methods, 7, 576-584, 10.4319/lom.2009.7.576, 2009.

Berg, P., Long, M. H., Huettel, M., Rheuban, J. E., McGlathery, K. J., Howarth, R. W., Foreman, K. H., Giblin, A. E., and Marino, R.: Eddy correlation measurements of oxygen fluxes in permeable sediments exposed to varying current flow and
330   light, Limnology and Oceanography, 58, 1329-1343, 10.4319/lo.2013.58.4.1329, 2013.

Berg, P., Reimers, C. E., Rosman, J. H., Huettel, M., Delgard, M. L., Reidenbach, M. A., and Ozkan-Haller, H. T.: Technical note: Time lag correction of aquatic eddy covariance data measured in the presence of waves, Biogeosciences, 12, 6721-6735, 10.5194/bg-12-6721-2015, 2015.

Bernardi, A., Nikolaou, A., Meneghesso, A., Chachuat, B., Morosinotto, T., and Bezzo, F.: A Framework for the Dynamic
335   Modelling of PI Curves in Microalgae, in: 12th International Symposium on Process Systems Engineering and 25th European Symposium on Computer Aided Process Engineering, Pt C, edited by: Gernaey, K. V., Huusom, J. K., and Gani, R., Computer Aided Chemical Engineering, 2483-2488, 2015.

Boucher, G., Clavier, J., and Garrigue, C.: Oxygen and carbon-dioxide fluxes at the water-sediment interface of a tropical lagoon, Marine Ecology Progress Series, 107, 185-193, 10.3354/meps107185, 1994.

340   Boucher, G., Clavier, J., Hily, C., and Gattuso, J. P.: Contribution of soft-bottoms to the community metabolism (primary production and calcification) of a barrier reef flat (Moorea, French Polynesia), Journal of Experimental Marine Biology and Ecology, 225, 269-283, 10.1016/s0022-0981(97)00227-x, 1998.

Brodersen, K. E., Lichtenberg, M., Ralph, P. J., Kuhl, M., and Wangpraseurt, D.: Radiative energy budget reveals high photosynthetic efficiency in symbiont-bearing corals, Journal of the Royal Society Interface, 11, 10.1098/rsif.2013.0997, 2014.

345   Chipman, L., Berg, P., and Huettel, M.: Benthic Oxygen Fluxes Measured by Eddy Covariance in Permeable Gulf of Mexico Shallow-Water Sands, Aquatic Geochemistry, 22, 529-554, 10.1007/s10498-016-9305-3, 2016.

Clavier, J., and Garrigue, C.: Annual sediment primary production and respiration in a large coral reef lagoon (SW New Caledonia), Marine Ecology-Progress Series, 191, 79-89, 1999.

Cyronak, T., Santos, I. R., McMahon, A., and Eyre, B. D.: Carbon cycling hysteresis in permeable carbonate sands over a diel
350   cycle: Implications for ocean acidification, Limnology and Oceanography, 58, 131-143, 10.4319/lo.2013.58.1.0131, 2013.

Deschaseaux, E., Stoltenberg, L., Hrebien, V., Koveke, E. P., Toda, K., and Eyre, B. D.: Dimethylsulfide (DMS) fluxes from permeable coral reef carbonate sediments, Marine Chemistry, 208, 1-10, 10.1016/j.marchem.2018.11.008, 2019.

Donis, D., Holtappels, M., Noss, C., Cathalot, C., Hancke, K., Polsenaere, P., Wenzhoefer, F., Lorke, A., Meysman, F. J. R., Glud, R. N., and McGinnis, D. F.: An Assessment of the Precision and Confidence of Aquatic Eddy Correlation Measurements,
355   Journal of Atmospheric and Oceanic Technology, 32, 642-655, 10.1175/jtech-d-14-00089.1, 2015.

Donis, D., McGinnis, D. F., Holtappels, M., Felden, J., and Wenzhoefer, F.: Assessing benthic oxygen fluxes in oligotrophic deep sea sediments (HAUSGARTEN observatory), Deep-Sea Research Part I-Oceanographic Research Papers, 111, 1-10, 10.1016/j.dsr.2015.11.007, 2016.

Eyre, B. D., Glud, R. N., and Patten, N.: Mass coral spawning: A natural large-scale nutrient addition experiment, Limnology and Oceanography, 53, 997-1013, 2008.

Eyre, B. D., Santos, I. R., and Maher, D. T.: Seasonal, daily and diel N-2 effluxes in permeable carbonate sediments, Biogeosciences, 10, 2601-2615, 10.5194/bg-10-2601-2013, 2013.

Eyre, B. D., Cyronak, T., Drupp, P., De Carlo, E. H., Sachs, J. P., and Andersson, A. J.: Coral reefs will transition to net dissolving before end of century, Science, 359, 908-911, 10.1126/science.aao1118, 2018.

Fan, S. M., Wofsy, S. C., Bakwin, P. S., Jacob, D. J., and Fitzjarrald, D. R.: Atmosphere-biosphere exchange of co2 and o3 in the central-amazon-forest, Journal of Geophysical Research-Atmospheres, 95, 16851-16864, 10.1029/JD095iD10p16851, 1990.

Fogarty, N. D., and Marhaver, K. L.: Coral spawning, unsynchronized, Science, 365, 987-988, 10.1126/science.aay7457, 2019.

Glud, R. N.: Oxygen dynamics of marine sediments, Marine Biology Research, 4, 243-289, 10.1080/17451000801888726, 2008.

Glud, R. N., Eyre, B. D., and Patten, N.: Biogeochemical responses to mass coral spawning at the Great Barrier Reef: Effects on respiration and primary production, Limnology and Oceanography, 53, 1014-1024, 2008.

Glud, R. N., Berg, P., Hume, A., Batty, P., Blicher, M. E., Lennert, K., and Rysgaard, S.: Benthic O-2 exchange across hard-bottom substrates quantified by eddy correlation in a sub-Arctic fjord, Marine Ecology Progress Series, 417, 1-12, 10.3354/meps08795, 2010.

Grenz, C., Denis, L., Boucher, G., Chauvaud, L., Clavier, J., Fichez, R., and Pringault, O.: Spatial variability in Sediment Oxygen Consumption under winter conditions in a lagoonal system in New Caledonia (South Pacific), Journal of Experimental Marine Biology and Ecology, 285, 33-47, 10.1016/s0022-0981(02)00518-x, 2003.

Grenz, C., Denis, L., Pringault, O., and Fichez, R.: Spatial and seasonal variability of sediment oxygen consumption and nutrient fluxes at the sediment water interface in a sub-tropical lagoon (New Caledonia), Marine Pollution Bulletin, 61, 399-412, 10.1016/j.marpolbul.2010.06.014, 2010.

Harris, D. L., Vila-Concejo, A., Webster, J. M., and Power, H. E.: Spatial variations in wave transformation and sediment entrainment on a coral reef sand apron, Marine Geology, 363, 220-229, 10.1016/j.margeo.2015.02.010, 2015.

Holtappels, M., Glud, R. N., Donis, D., Liu, B., Hume, A., Wenzhofer, F., and Kuypers, M. M. M.: Effects of transient bottom water currents and oxygen concentrations on benthic exchange rates as assessed by eddy correlation measurements, Journal of Geophysical Research-Oceans, 118, 1157-1169, 10.1002/jgrc.20112, 2013.

Hopkinson, C. S., and Smith, E. M.: Estuarine respiration: an overview of benthic, pelagic, and whole system respiration, in: Respiration in Aquatic Ecosystems (Oxford Biology) (Hardcover)
, edited by: Williams, P. d. G. a. P., Oxford University Press, Oxford Scholarship Online, 122-146, 2005.

390 Horton, N. A., and Pokrajac, D.: Onset of turbulence in a regular porous medium: An experimental study, Physics of Fluids, 21, 10.1063/1.3091944, 2009.

Huettel, M., and Gust, G.: Solute Release Mechanisms From Confined Sediment Cores In Stirred Benthic Chambers and Flume Flows, Marine Ecology Progress Series, 82, 187-197, 1992.

Huettel, M., Berg, P., and Kostka, J. E.: Benthic Exchange and Biogeochemical Cycling in Permeable Sediments, Annual
395 Review of Marine Science, Vol 6, 6, 23-51, 10.1146/annurev-marine-051413-012706, 2014.

Huettel, M., Berg, P., and Merikhi, A.: Technical note: Measurements and data analysis of sediment-water oxygen flux using a new dual-optode eddy covariance instrument, Biogeosciences, 17, 4459-4476, 10.5194/bg-17-4459-2020, 2020.

Hughes, T. P., Anderson, K. D., Connolly, S. R., Heron, S. F., Kerry, J. T., Lough, J. M., Baird, A. H., Baum, J. K., Berumen, M. L., Bridge, T. C., Claar, D. C., Eakin, C. M., Gilmour, J. P., Graham, N. A. J., Harrison, H., Hobbs, J. P. A., Hoey, A. S.,
400 Hoogenboom, M., Lowe, R. J., McCulloch, M. T., Pandolfi, J. M., Pratchett, M., Schoepf, V., Torda, G., and Wilson, S. K.: Spatial and temporal patterns of mass bleaching of corals in the Anthropocene, Science, 359, 80-+, 10.1126/science.aan8048, 2018.

Janssen, F., Faerber, P., Huettel, M., Meyer, V., and Witte, U.: Pore-water advection and solute fluxes in permeable marine sediments (I): Calibration and performance of the novel benthic chamber system Sandy, Limnology and Oceanography, 50,
405 768-778, 2005.

Jantzen, C., Schmidt, G. M., Wild, C., Roder, C., Khokiattiwong, S., and Richter, C.: Benthic Reef Primary Production in Response to Large Amplitude Internal Waves at the Similan Islands (Andaman Sea, Thailand), Plos One, 8, 10.1371/journal.pone.0081834, 2013.

Jouybari, N. F., Lundstrom, T. S., and Hellstrom, J. G. I.: Investigation of Hydrodynamic Dispersion and Intra-pore Turbulence
410 Effects in Porous Media, Transport in Porous Media, 131, 739-765, 10.1007/s11242-019-01365-0, 2020.

Koopmans, D., Holtappels, M., Chennu, A., Weber, M., and de Beer, D.: High Net Primary Production of Mediterranean Seagrass (Posidonia oceanica) Meadows Determined With Aquatic Eddy Covariance, Frontiers in Marine Science, 7, 10.3389/fmars.2020.00118, 2020.

Kuwae, T., Kamio, K., Inoue, T., Miyoshi, E., and Uchiyama, Y.: Oxygen exchange flux between sediment and water in an
415 intertidal sandflat, measured in situ by the eddy-correlation method, Marine Ecology Progress Series, 307, 59-68, 10.3354/meps307059, 2006.

Laursen, A. E., and Seitzinger, S. P.: The role of denitrification in nitrogen removal and carbon mineralization in Mid-Atlantic Bight sediments, Continental Shelf Research, 22, 1397-1416, 2002.

Lee, S. K., and Cheung, K. F.: Laminar and turbulent bottom boundary layer induced by nonlinear water waves, Journal of
420 Hydraulic Engineering-Asce, 125, 631-644, 10.1061/(asce)0733-9429(1999)125:6(631), 1999.

Lee, X., Massman, W., and Law, B. A.: Handbook of micrometeorology : a guide for surface flux measurement and analysis, Springer, 2004.

Long, M. H., Berg, P., de Beer, D., and Zieman, J. C.: In Situ Coral Reef Oxygen Metabolism: An Eddy Correlation Study, Plos One, 8, 10.1371/journal.pone.0058581, 2013.

425 Long, M. H.: Aquatic biogeochemical eddy covariance fluxes in the presence of waves., Journal of Geophysical Research: Oceans, 126, e2020JC016637, 10.1029/2020JC016637, 2021.

Lorke, A., McGinnis, D. F., and Maeck, A.: Eddy-correlation measurements of benthic fluxes under complex flow conditions: Effects of coordinate transformations and averaging time scales, Limnology and Oceanography-Methods, 11, 425-437, 10.4319/lom.2013.11.425, 2013.

430 Lorrai, C., McGinnis, D. F., Berg, P., Brand, A., and Wuest, A.: Application of Oxygen Eddy Correlation in Aquatic Systems, Journal of Atmospheric and Oceanic Technology, 27, 1533-1546, 10.1175/2010jtecho723.1, 2010.

Marcelino, L. A., Westneat, M. W., Stoyneva, V., Henss, J., Rogers, J. D., Radosevich, A., Turzhitsky, V., Siple, M., Fang, A., Swain, T. D., Fung, J., and Backman, V.: Modulation of Light-Enhancement to Symbiotic Algae by Light-Scattering in Corals and Evolutionary Trends in Bleaching, Plos One, 8, 10.1371/journal.pone.0061492, 2013.

435 Massman, W. J., and Lee, X.: Eddy covariance flux corrections and uncertainties in long-term studies of carbon and energy exchanges, Agricultural and Forest Meteorology, 113, 121-144, 10.1016/s0168-1923(02)00105-3, 2002.

McGinnis, D. F., Berg, P., Brand, A., Lorrai, C., Edmonds, T. J., and Wueest, A.: Measurements of eddy correlation oxygen fluxes in shallow freshwaters: Towards routine applications and analysis, Geophysical Research Letters, 35, 10.1029/2007gl032747, 2008a.

440 McGinnis, D. F., Berg, P., Brand, A., Lorrai, C., Edmonds, T. J., and Wuest, A.: Measurements of eddy correlation oxygen fluxes in shallow freshwaters: Towards routine applications and analysis, Geophysical Research Letters, 35, 10.1029/2007gl032747, 2008b.

McGinnis, D. F., Sommer, S., Lorke, A., Glud, R. N., and Linke, P.: Quantifying tidally driven benthic oxygen exchange across permeable sediments: An aquatic eddy correlation study, Journal of Geophysical Research-Oceans, 119, 6918-6932, 445 10.1002/2014jc010303, 2014.

Merikhi, A., Berg, P., Meyer, V., and Huettel, M.: Jet-nozzle method for measuring response times of scalar sensors used in liquids and gases, Limnology and Oceanography-Methods, 16, 475-483, 10.1002/lom3.10259, 2018.

Middelburg, J. J., Duarte, C. M., and Gattuso, J. P.: Respiration in coastal benthic communities, in: Respiration in Aquatic Ecosystems (Oxford Biology) (Hardcover)

450 , edited by: Williams, P. d. G. a. P., Oxford University Press, Oxford Scholarship Online, 206-225, 2005.

Pawlik, J. R., Burkepile, D. E., and Thurber, R. V.: A Vicious Circle? Altered Carbon and Nutrient Cycling May Explain the Low Resilience of Caribbean Coral Reefs, Bioscience, 66, 470-476, 10.1093/biosci/biw047, 2016.

Rasheed, M., Wild, C., Franke, U., and Huettel, M.: Benthic photosynthesis and oxygen consumption in permeable carbonate sediments at Heron Island, Great Barrier Reef, Australia, Estuarine Coastal and Shelf Science, 59, 139-150, 2004.

455 Reimers, C. E., Oezkan-Haller, H. T., Berg, P., Devol, A., McCann-Grosvenor, K., and Sanders, R. D.: Benthic oxygen consumption rates during hypoxic conditions on the Oregon continental shelf: Evaluation of the eddy correlation method, Journal of Geophysical Research-Oceans, 117, 10.1029/2011jc007564, 2012.

Reimers, C. E., Ozkan-Haller, H. T., Albright, A. T., and Berg, P.: Microelectrode Velocity Effects and Aquatic Eddy Covariance Measurements under Waves, Journal of Atmospheric and Oceanic Technology, 33, 263-282, 10.1175/jtech-d-15-

460 0041.1, 2016.

Rheuban, J. E., Berg, P., and McGlathery, K. J.: Multiple timescale processes drive ecosystem metabolism in eelgrass (Zostera marina) meadows, Marine Ecology Progress Series, 507, 1-13, 10.3354/meps10843, 2014.

Santos, I. R., Glud, R. N., Maher, D., Erler, D., and Eyre, B. D.: Diel coral reef acidification driven by porewater advection in permeable carbonate sands, Heron Island, Great Barrier Reef, Geophysical Research Letters, 38, 10.1029/2010gl046053, 2011.

465 Sleath, J. F. A.: STABILITY OF LAMINAR-FLOW AT SEABED, Journal of the Waterways Harbors and Coastal Engineering Division-Asce, 100, 105-122, 1974.

Stuart-Smith, R. D., Brown, C. J., Ceccarelli, D. M., and Edgar, G. J.: Ecosystem restructuring along the Great Barrier Reef following mass coral bleaching, Nature, 560, 92-+, 10.1038/s41586-018-0359-9, 2018.

Werner, U., Blazejak, A., Bird, P., Eickert, G., Schoon, R., Abed, R. M. M., Bissett, A., and de Beer, D.: Microbial

470 photosynthesis in coral reef sediments (Heron Reef, Australia), Estuarine Coastal and Shelf Science, 76, 876-888, 10.1016/j.ecss.2007.08.015, 2008.

Wild, C., Huettel, M., Klueter, A., Kremb, S. G., Rasheed, M. Y. M., and Jorgensen, B. B.: Coral mucus functions as an energy carrier and particle trap in the reef ecosystem, Nature, 428, 66-70, 2004a.

Wild, C., Rasheed, M., Werner, U., Franke, U., Johnstone, R., and Huettel, M.: Degradation and mineralization of coral mucus

475 in reef environments, Marine Ecology-Progress Series, 267, 159-171, 2004b.

Wild, C., Tollrian, R., and Huettel, M.: Rapid recycling of coral mass-spawning products in permeable reef sediments, Marine Ecology-Progress Series, 271, 159-166, 2004c.

Wild, C., Rasheed, M., Jantzen, C., Cook, P., Struck, U., Huettel, M., and Boetius, A.: Benthic metabolism and degradation of natural particulate organic matter in carbonate and silicate reef sands of the northern Red Sea, Marine Ecology-Progress Series,

480 298, 69-78, 2005a.

Wild, C., Woyt, H., and Huettel, M.: Influence of coral mucus on nutrient fluxes in carbonate sands, Marine Ecology-Progress Series, 287, 87-98, 2005b.

Wild, C., Laforsch, C., and Huettel, M.: Detection and enumeration of microbial cells within highly porous calcareous reef sands, Marine and Freshwater Research, 57 415–420, 2006.

485 Yahel, R., Yahel, G., and Genin, A.: Daily cycles of suspended sand at coral reefs: A biological control, Limnology and Oceanography, 47, 1071-1083, 10.4319/lo.2002.47.4.1071, 2002.